

Is surface melting a surface phase transition?

Paul J. M. Bastiaansen* and Hubert J. F. Knops
*Institute for Theoretical Physics, University of Nijmegen,
Toernooiveld, 6525 ED Nijmegen, The Netherlands*

Abstract

Monte Carlo or Molecular Dynamics calculations of surfaces of Lennard-Jones systems often indicate, apart from a gradual disordering of the surface called surface melting, the presence of a phase transition at the surface, but cannot determine the nature of the transition. In the present paper, we provide for a link between the continuous Lennard-Jones system and a lattice model. We apply the method for the (001) surface of a Lennard-Jones fcc structure pertaining to Argon. The corresponding lattice model is a Body Centered Solid on Solid model with an extended range of interaction, showing in principle rough, flat and disordered flat phases. We observe that entropy effects considerably lower the strength of the effective couplings between the atoms. The Argon (001) face is shown to exhibit a phase transition at $T = 70.5 \pm 0.5$ K, and we identify this transition as roughening. The roughening temperature is in good correspondence with experimental results for Argon.

PACS numbers:

68.35.Rh – Surfaces and interfaces - phase transitions and critical phenomena

82.65.Dp – Thermodynamics of surfaces and interfaces

64.60.Cn – Order-disorder and statistical mechanics of model systems

I. INTRODUCTION AND MOTIVATION

Surface melting, in particular of simple Lennard-Jones systems like Argon, is well understood as the wetting of the solid by its own melt. A liquid-like layer appears between the solid and the vapor, and the thickness of this layer increases with temperature. Theoretically, the phenomenon is described with a Landau theory¹ and, more recently, using a Density Functional approach.²

It is clear that the atoms in the liquid-like layer between the bulk and the vapor are influenced by the presence of the underlying crystal. Therefore, the layer should be regarded as a quasi-liquid exhibiting properties that are intermediate between those of the solid and the bulk liquid. To decide upon surface melting in Molecular Dynamics calculations, one usually considers the behavior of an appropriate quantity like, e.g., the parallel integrated density

$$\rho(z) = \int dx dy \rho(\mathbf{r}), \quad (1)$$

where z is the direction transversal to the interface, and

$$\rho(\mathbf{r}) = \sum_j \delta(\mathbf{r} - \mathbf{r}_j) \quad (2)$$

with j running over all particle positions \mathbf{r}_j . This $\rho(z)$ shows sharp peaks in the bulk, while in the case of surface melting the peaks broaden when z approaches the interface. The onset of the quasi-liquid layer then can be defined, more or less arbitrarily, by a suitable broadening of the peaks. In the case of complete surface melting, the thickness l of the quasi-liquid layer diverges as the temperature approaches the triple point temperature T_3 of the bulk. As follows from the wetting theory in the case of Lennard-Jones systems, the thickness of the layer increases with temperature as a power law, and this is experimentally confirmed.³

The wetting theory concentrates on this parameter $\rho(z)$ but cannot give information concerning the atomic structure in the few top layers when the triple point T_3 is approached. Specifically, one could ask whether the top layer does exhibit a genuine surface phase transition at a temperature $T_c < T_3$. It is possible that the phenomenon of surface melting is a gradual process of the thickening of the quasi-liquid layer, with no surface phase transition at all. But since the wetting theory fails to detect a genuine two-dimensional transition, it could well be that surface melting is accompanied by a surface phase transition which takes place at a temperature lower than the triple point temperature. Such a transition could either be a roughening transition, involving the transversal degrees of freedom, or a two-dimensional ‘melting’ transition involving the in-plane degrees of freedom. The connection between surface melting and possible surface phase transitions is as yet not understood.

One of the difficulties in addressing this question is the definition of a suitable order parameter. Clearly, the parallel integrated density cannot be an order parameter.

Van der Eerden *et al.*⁴⁻⁶ proposed the surface shear modulus as an order parameter for a surface phase transition accompanying surface melting. In a Monte Carlo simulation of the (001) face of a Lennard-Jones fcc structure, they found indications for such a transition,

but, as is in general the case with such calculations, no information regarding the nature of this transition was obtained. It is this question we want to address in this paper.

At the outset it should be clear that a ‘melting’ transition associated with the lateral degrees of freedom of the top layer cannot be a two-dimensional melting transition of the Nelson-Halperin-Young type.^{7–10} This is because the bulk under the top layer provides a substrate potential which is commensurate to the top layer. Such a potential is known^{7,11} to be relevant in the renormalization group sense. It is therefore more appropriate to adopt a lattice model, with the lattice dictated by the substrate. Judging from the Monte Carlo data from simulations on Lennard-Jones interfaces well below the triple point,^{5,6,12} neglecting overhangs and vacancies is not a serious approximation. Accepting this approximation, one arrives at a Solid On Solid (SOS) model.

It is by now well known that, if one allows for more than nearest neighbor interactions, the phase diagram of these SOS models can be very rich.¹³ Possible phase transitions include roughening,¹⁴ preroughening,¹⁵ and deconstruction.¹⁶ The preroughening and deconstruction transitions are from a flat or reconstructed phase into a so-called Disordered Flat (DOF) phase, in which the surface is disordered but remains flat on average. Typically such a transition can occur when the next nearest neighbor couplings become strong as compared to the nearest neighbor couplings.

The couplings in the lattice model are effective couplings to be calculated from the original continuous Lennard-Jones system. In the context of lattice models, one usually just estimates the values of the couplings, e.g. by counting the ‘broken bonds’. In deriving a lattice model from the continuous Lennard-Jones system, however, one should integrate the continuous degrees of freedom, thereby obtaining effective couplings which typically contain a gain term due to the increased potential energy (the broken bond), but also a loss term due to an increase of entropy, since a particle in a cell adjacent to a vacant cell has more freedom to move. This effect lowers in particular the strength of the nearest neighbor coupling.

It is the goal of the present work to actually calculate the effective couplings for a lattice model, pertaining to the (001) surface of a Lennard-Jones fcc structure, and to analyze this model. In this way we can determine the nature of a possible transition at this interface, which is not feasible with Monte Carlo or Molecular Dynamics calculations. We use a Lennard-Jones potential appropriate for Argon, calculate the effective couplings of the corresponding lattice model by integrating the continuous degrees of freedom of the Lennard-Jones system, and analyze the resulting SOS model.

This paper is organized as follows. In Sec. II we describe the method used to arrive at the lattice model, starting from the Lennard-Jones system. In Sec. III we carry out the calculations and present the results. In Sec. IV we give a description of the SOS model that pertains to the (001) interface and present the phase diagram of the model. We end with a conclusion. Several checks, validating the approximations and testing the procedures, are addressed in the Appendix.

II. OUTLINE OF THE METHOD

Deriving the lattice model from the continuous Lennard-Jones system requires a number of steps. First we have to establish a cell description of the surface. We notice from the

simulations of Broughton and Gilmer¹⁷ that there is a considerable range of temperatures up to about 75 K where the top layer of the (001) face shows already an irregular pattern while the atoms in all other layers are close to their average positions and still behave as bulk atoms. Note that the triple point of Argon found by Broughton and Gilmer is at $T_3 = 82.7$ K (compared to the experimental value¹⁸ of $T_3 = 83.810$ K). Concentrating on a temperature range up to $T = 75$ K, it is a good approximation to neglect correlations between the top layer and the bulk, thus treating the bulk in a mean field manner. We use Monte Carlo simulations to evaluate the average bulk lattice distance $a(T)$ as a function of temperature. This distance $a(T)$ then defines the cell dimensions of the surface cells. For the (001) face, these cells are rectangular blocks with dimension $\frac{1}{2}\sqrt{2} a(T)$ centered around the average atom position. The height of the cell is chosen such that the average potential at the top of the cell is negligible.

As the substrate potential is caused by layers under the surface which, as follows from the calculations of Broughton and Gilmer, behave as bulk layers, we can calculate the substrate potential, present in the cells, in a bulk simulation.

Having defined the cells with the substrate potential, we can evaluate the effective (temperature dependent) couplings in the lattice model, arising from the continuous Lennard-Jones system. Therefore we choose several different surface configurations with some cells occupied and some empty, and calculate the corresponding free energies by integrating the continuous degrees of freedom of the atoms in their cells. Comparing this free energy with the free energy of the fully occupied surface, we arrive at a lattice model of the (001) surface, with the only degrees of freedom left being discrete and describing whether or not an atom is present on its site.

In this way one can arrive in principle at an exact representation of the continuous system as a lattice model, but in practice one only considers effective couplings extending over a limited range. Instead of sticking to the language of atom-atom couplings, we will express the energy of a configuration in terms of elementary step and kink configurations at the surface. Limiting the range of the couplings to the next-nearest neighbor distance, the four elementary step and kink configurations are those depicted in Fig. 1. We calculate the free energies of nine different surface configurations and express the free energies as good as possible in terms of the vertex free energies F_1 to F_4 . The accuracy of this match gives an estimate of the error in neglecting couplings with a range beyond the next-nearest neighbor distance.

The nine different configurations are chosen to fit on a strip of $3 \times \infty$ cells which is periodically repeated. This makes it possible to find their surface free energies by a transfer matrix method.

The final step in the procedure is to analyze the resulting SOS model. Actually the appropriate SOS model for a (001) face of an fcc structure is the Body Centered Solid On Solid (BCSOS) model, which is directly related to the six vertex model¹⁹ with an extended range of the interactions. A section of the phase diagram of this model has recently been investigated by us²⁰ showing that the inclusion of next nearest neighbor interactions indeed is capable of stabilizing a DOF phase. We use the same method as described in this reference to explore the occurrence of a two-dimensional phase transition along the temperature path from 50 K up to 75 K in the phase diagram.

III. EFFECTIVE STEP ENERGIES

We derive the BCSOS model from the continuous Lennard-Jones system by calculating the (temperature dependent) effective step energies F_1 to F_4 from Fig. 1. The system under study is a Lennard-Jones fcc structure pertaining to Argon. The precise potential we use is the same as that used in Ref. 5,

$$V(r) = 4.569\varepsilon \left[\left(\frac{r}{\sigma}\right)^{-12} - \left(\frac{r}{\sigma}\right)^{-6} \right] \exp\left(\frac{0.25\sigma}{r - 2.5\sigma}\right) \quad \text{for } r < 2.5\sigma, \quad (3)$$

and vanishes for $r \geq 2.5\sigma$. To model Argon, the following values are used:

$$\frac{\varepsilon}{k} = 119.8 \text{ K} \quad (4)$$

$$\sigma = 0.33 \text{ nm}. \quad (5)$$

These values define the scale of our calculations, and can be used to transfer the numerical results in terms of reduced units. As our calculations particularly pertain to Argon, we choose to express the results in terms of SI units.

Bulk simulations, used for establishing the cell description of the surface, are treated in Sec. III A. In Sec. III B, we use a transfer matrix method to calculate the effective step free energies. Results are presented in Sec. III C

A. Bulk simulations

This section deals with computing the effective substrate potential to which the surface atoms are subject. The substrate potential arises from the bulk. The main assumption regarding this section is that there are only two types of atoms: bulk atoms and surface atoms. Surface atoms are those in the top layer; the remainder are bulk atoms. The assumption is that atoms close to the surface are not affected by the surface; the substrate potential in the surface layer thus is dictated exclusively by the behavior of the bulk and can be determined in a bulk simulation.

Therefore we define a bulk system, consisting of 972 atoms in an fcc configuration with periodic boundary conditions in every direction. It is oriented such that a (001) layer of the configuration lies horizontally. We choose one (001) layer of atoms from this configuration. The substrate potential at a certain point in this layer now arises from all atoms *under* this layer.

Extracting the desired potential pattern consists of three steps: first we have to compute the equilibrium volumes of the system at several temperatures and fixed external pressure. In a next simulation, we fix this equilibrium volume and compute the average positions of each of the atoms. These average positions together with the equilibrium lattice parameter determines the cells corresponding to each of the atoms. These cells are rectangular blocks, and the center of the cell is the averaged position of the corresponding atom. We can now rerun the second simulation (i.e. generating the same configurations), but now with the average atom positions known beforehand. In the cells, we compute the average substrate potential pattern arising from all atoms *under* the layer where the cell is part of. As, due

to translational invariance, all cells are equivalent, we can average all measured potential patterns, thus giving rise to one average pattern in a cell. This pattern is the desired substrate potential.

We do calculations in the temperature range of 50 to 75 K, still well below the triple point of Argon. We will use an external pressure $P = 0$ for our simulations, which is, strictly spoken, not correct, as we do have to consider the system in equilibrium with its vapor. The vapor pressure, however, will be very low, and the properties of a solid are relatively insensitive to pressure. We regard choosing $P = 0$ as a good approximation.

The results of the volume calculations, expressed as nearest neighbor distances and compared to those of Broughton and Gilmer,²¹ are shown in Fig. 2 and show a close correspondence. The thermal cubic coefficient of expansion α is given by

$$\alpha = \frac{1}{V} \left(\frac{\partial V}{\partial T} \right)_P. \quad (6)$$

We find at $T = 60$ K a value of $\alpha = 2.15 \times 10^{-3} \text{ K}^{-1}$, as compared to the result of Broughton and Gilmer²¹ calculated from their polynomial fit of the nearest neighbor distance, $\alpha = 2.04 \times 10^{-3} \text{ K}^{-1}$, and the result of Van der Eerden *et al.*,⁶ $\alpha = 1.95 \times 10^{-3} \text{ K}^{-1}$. Note that Broughton and Gilmer use a slightly different Lennard-Jones potential.

Having carried out the volume measurements, we can start measuring the potential pattern. We perform the simulations with a fixed volume V , and fix this volume at its equilibrium value as described above. In the first simulation, we calculate the average position of all atoms to determine the centers of the cells. During the simulation, we store the generated configurations which we used for measurements, in order to use them again in the next simulation.

Then we define in every cell a fine grid consisting of $21 \times 21 \times 21$ points, at which we measure the average potential. In course of our simulations, it turned out that we had to extend the grid above the cell, because we wanted to measure the potential up to a height where it becomes negligible. The defined grid therefore has a height of 3/2 of the height of the bulk cell. In the simulation, we use the already stored configurations. We measure the substrate potential in each of the 9261 points of the grid, and average over all cells. During the simulation, we have to check whether the cell picture makes sense. It does, provided the atoms remain in their cell during the simulation. We check this for all atoms, and it turns out that not a single atom moves out of its cell.

As expected, the fluctuations in the potential are relatively large, which means that we have to simulate long. We used 800 measurements, with 3000 generated configurations between each measurement.

B. Transfer matrix calculations

The first step in our procedure, the determination of the substrate potential pattern, has now been carried out. We will use this potential pattern as a mean field, to which the surface atoms are subject. However, we have to check whether this mean field approximation makes sense, and indeed will do so using different methods. The checks will be treated in the Appendix.

Our task is to integrate the continuous degrees of freedom of the surface atoms in their cells. We will do this using a transfer matrix calculation, which, in principle, gives exact results. We have, however, to discretize as a continuous integration is not possible. If we choose a surface in which one row consists of N cells with L grid points per cell, the dimension of the transfer matrix is $L^N \times L^N$. The boundary conditions are periodic: the row is closed at the ends.

The substrate potential pattern consists of 9261 points, which means that now $L = 9261$. This yields a much too large dimension of the transfer matrix. Therefore, we have to reduce drastically the number of points L . We choose $L = 25$ and $N = 3$, yielding a linear dimension of the transfer matrix $L^N = 15625$. We will distribute the 25 points in the cell as efficiently as possible, by choosing the grid points unevenly distributed in the cell and making the pattern two-dimensional. Both approximations, reducing the number of points and making the grid two-dimensional, will be validated.

The Hamiltonian of our surface system is

$$H = \sum_i V_{\text{subs}}(\mathbf{r}_i) + \sum_{i,j} V_{\text{LJ}}(|\mathbf{r}_i - \mathbf{r}_j|), \quad (7)$$

where the indices run over all particles, V_{subs} is the substrate potential and V_{LJ} is the Lennard-Jones potential from Eq. (3). V_{LJ} is cut off such that only nearest and next nearest neighbors interact; otherwise the transfer matrix dimension increases.

Making the grid two-dimensional means that we ignore the dependence of $V_{\text{LJ}}(|\mathbf{r}_i - \mathbf{r}_j|)$ on z_i and z_j . The z integration can then be done directly in the partition function. This is done by just adding all potential patterns with different z coordinates, and multiplying the corresponding Boltzmann weights by the height of the grid.

Then we choose the $L = 25$ grid points as efficiently as possible. The idea is as follows: the lower the Boltzmann weight in a certain point of the cell, the less relevant is the corresponding area in the partition function, so the distribution can be less dense in that area. On the other hand, points have to be dense in those areas where the Boltzmann weights are high. Grosso modo this means that the distribution of points should be more dense in the center of the cell and less dense towards the edges. We choose the location of the points according to Fig. 3. The figure depicts the two-dimensional cell with 25 points, each point being in its corresponding domain. The points are in the middle (the ‘center of mass’) of their domain. The domains are defined by the three variables R_1 , R_2 and ϕ .

We choose the grid points as in the figure, and we assign a Boltzmann weight to each of the domains. Consider one domain with the original (dense) grid points being in it. To obtain the correct Boltzmann weight, we first determine the average potential V in that domain, calculate the corresponding Boltzmann weight $W = \exp(-V)$ and multiply this with the area of the domain. This is the Boltzmann weight we are going to use in the transfer matrix calculation. To obtain the most efficient distribution of points, we fix the variables R_1 , R_2 and ϕ such that the Boltzmann weights multiplied by their corresponding area, are (almost) equal to each other. A lower Boltzmann weight then automatically corresponds to a larger domain, and the resulting weights are equally relevant. Theoretically, they are all exactly equal so we could leave them out, but in practice we do not succeed in fixing the parameters such that the weights are exactly equal, so we choose to leave them where they are.

The calculated coordinates of the 25 grid points, together with the associated Boltzmann weights, are used as input for the transfer matrix calculations. We calculate the free energy

of several different surface configurations, each consisting of occupied and empty cells. We choose them such as to have much variety in the configurations, and we choose them overcomplete for determining the vertex free energies F_1 to F_4 from Fig. 1. The configurations we choose are depicted in Fig. 4, where the pictures are understood to extend to infinity at the right and left ends. The ‘rows’ of the transfer matrix are depicted vertically; the direction of transfer is horizontal. We have to define a different transfer matrix for each different pair of rows; transferring from a row with, say, three occupied cells to a row with two occupied cells corresponds to a transfer matrix with dimension $25^3 \times 25^2$.

Let us define the different transfer matrices by, for example, $T(110|111)$, where the digits refer to the cells. A digit 0 indicates that the corresponding cell is empty, a 1 that it is occupied. So $T(110|111)$ is the transfer matrix between a left row having its lower two cells occupied, and a right row having all cells occupied. Note that none of the transfer matrices is symmetric and that most of them are not even square matrices.

First we calculate the largest eigenvalue λ_{\max} and the corresponding left and right eigenvectors $\langle\psi|$ and $|\psi\rangle$ of the ‘full’ transfer matrix $T(111|111)$. The free energy of one particle in a fully occupied surface is $F = -\frac{1}{3} \ln \lambda_{\max}$. Now the partition function of, say, configuration number 9 in Fig. 4 is

$$Z = \frac{1}{\lambda_{\max}^2} \langle\psi| T(111|101) T(101|010) T(010|111) |\psi\rangle. \quad (8)$$

The eigenvectors are normalized as $\langle\psi|\psi\rangle = 1$. Note that we divide by λ_{\max}^2 , because we want to subtract the free energy of a fully occupied surface consisting of precisely as many atoms as configuration number 9. Similar expressions are used for the other surface configurations.

By calculating $F = -\ln Z$ we now have the free energies of all different surface configurations. We want to express those free energies in terms of step configurations at the surface. The step configurations we use are those possible at a vertex (the meeting point of four cells) and are depicted in Fig. 1. The fifth possible vertex is the vertex with no steps; it carries free energy 0. The nine free energies of the surface configurations of Fig. 4 are redundant for determining the values of the free energies F_1 to F_4 . We calculate F_j using a best fit method. Re-expressing the free energies of the nine surface configurations in terms of these vertex free energies indicates the quality of the fit.

Ideally, the F_j obey the following equation

$$\sum_{j=1}^4 T_{ij} F_j = A_i \quad (9)$$

where $A_i, i = 1 \dots 9$ is the free energy of surface configuration number i and T_{ij} expresses the number of times vertex j appears in configuration number i , that is

$$\tilde{T} = \begin{pmatrix} 6 & 8 & 8 & 6 & 6 & 2 & 4 & 4 & 2 \\ 0 & 2 & 2 & 4 & 0 & 4 & 4 & 2 & 0 \\ 0 & 2 & 2 & 0 & 4 & 4 & 4 & 4 & 4 \\ 0 & 0 & 0 & 0 & 0 & 0 & 0 & 1 & 2 \end{pmatrix}. \quad (10)$$

As argued before, the nine surface configurations are redundant for determining the free energies F_j , so Eq. (9) will have no solution. We will determine the F_j from this equation by introducing an error vector $\varepsilon_i, i = 1 \dots 9$ by

$$\sum_{j=1}^4 \frac{T_{ij} F_j}{A_i} = 1 + \varepsilon_i. \quad (11)$$

The components of ε_i describe the relative error of expressing the free energy of configuration number i in terms of the vertex free energies F_j . Minimizing $|\varepsilon|^2$ with respect to the vertex energies by solving

$$\frac{\partial |\varepsilon|^2}{\partial F_j} = 0 \quad (12)$$

yields the best values for F_j .

C. Results

The resulting values for F_1 to F_4 are plotted in Fig. 5. It turns out that expressing the surface free energies in terms of only these elementary configurations works well; the average percentual difference between the actual free energy and the free energy in terms of the F_j is about 1.2%, the maximum difference is 2.5%.

In lattice models, one usually estimates the interaction parameters by the energy of a broken bond. This energy is, in our case, the value of the Lennard-Jones potential at the equilibrium distance. One thus neglects the entropy gain that corresponds to the increased freedom of the moving atom. To see the strength of this effect, we choose one of the surface configurations, say configuration number 7, and plot its energy calculated from the broken bonds together with the actual free energy which results from our transfer matrix calculations. The plot is shown in Fig. 6. There turns out to be a considerable difference in the actual free energy and the energy calculated by counting the broken bonds. This difference is precisely the entropy which the atoms gain by moving in the cell, and, as expected, it increases with temperature.

To visualize the quality of the fit method described above, we also plot (in Fig. 6) the free energy of the configuration, but now re-expressed in terms of the vertex free energies F_j from Fig. 1. We see from the figure that expressing the free energy of the configuration in terms of the vertex energies is appropriate. We conclude that it is sufficient to consider only the vertex configurations 1 to 4, and that we do not need to consider more complex step configurations.

Finally, we want to check an hypothesis. We expected that the decrease in free energy of the surface with increasing temperature is mainly due to the increasing lattice parameter, and that it has little to do with the changing substrate potential pattern. Cell dimensions increase with temperature, which means that the atoms gain freedom and therefore entropy, while the potential pattern flattens a little but remains more or less the same. We can check this hypothesis by scaling the potential pattern at $T = 50$ K to the cell dimensions at $T = 70$ K, and calculating the free energies of the surface configurations. The results are tabulated in table I. We conclude that the increase of free energy with temperature can be explained for 98% by the increasing cell dimensions, and for roughly 2% by the flattening of the potential pattern. This confirms our hypothesis.

IV. THE LATTICE MODEL

We will now briefly discuss the lattice model following from our calculations. The model pertains to the (001) surface of an fcc crystal, which means that neighboring atoms always differ $\pm\frac{1}{2}a$ in height. A typical surface configuration is depicted in Fig. 7. The resulting lattice model is a BCSOS model, which can be mapped on a six vertex model.¹⁹

Consider a square lattice, where an arrow is placed on each of the bonds satisfying the so-called ice rule, which states that the number of incoming arrows at each vertex equals the number of outgoing arrows. The six possible arrow combinations at a vertex are depicted in Fig. 8. The rule for assigning heights to the lattice sites is that, when looking in the direction of an arrow, the higher atom is on the right. Fixing then the height of one of the sites, a vertex configuration is uniquely mapped onto a surface height configuration. The ice rule guarantees that the mapping is single valued.

The six vertex model in its original formulation assigns an energy to each of the six vertices, and has been completely solved.²² In our case, using the configurations and energies of Fig. 1, we have to take into account interactions between the vertices, which means that there is no exact solution of our model present. The energies which we assign to vertex configurations are visualized in Fig. 9, and result in a four-vertex interaction. Compare this figure to Fig. 1.

The model can be analyzed with transfer matrix calculations and standard analysis of Finite Size Scaling.²³ In another paper,²⁰ we analyze a section of the phase diagram of this BCSOS model and show that it contains in particular both a rough and a DOF phase. For a detailed account of the calculations we refer to this reference. Here, we apply the same method to determine the behavior of the Argon (001) surface, following from the values of the F_j in Fig. 5, but average the free energies F_2 and F_3 applying to inside and outside corners. Inequality of F_2 and F_3 breaks the particle-hole symmetry and cannot be present for a two body potential. The broken symmetry is present here because of entropy effects, which introduce effective many-body couplings. The effect will be to smear out the transition²⁴ but we neglect the difference here and use $(F_2 + F_3)/2$.

Our Finite Size Scaling analysis shows that the model exhibits a roughening transition at $T = 70.5 \pm 0.5$ K. Below this temperature, the surface is flat on average, with only now and then islands bounded by up or down steps. At higher temperatures, these islands start to grow, eventually diverging at the roughening temperature, where the step free energy vanishes.

In the more general analysis of the phase diagram of this BCSOS model, we assigned a Boltzmann weight W to a broken next nearest neighbor bond and a weight K to a broken third nearest neighbor bond. Note that nearest neighbors always differ $\pm\frac{1}{2}a$ in height. The phase diagram of the model is depicted in Fig. 10. In terms of W and K , the F_j would be

$$\beta F_1 = -\ln(WK^2) \quad (13)$$

$$\beta F_2 = -\ln(WK) \quad (14)$$

$$\beta F_3 = -\ln(WK) \quad (15)$$

$$\beta F_4 = -\ln(W^2). \quad (16)$$

The values of F_j that follow from our calculations of course can not be exactly expressed in terms of W and K ; we would need a higher dimensional parameter space. However, the

phase diagram gives an indication of where the Argon (001) surface is located with respect to the DOF and the rough phase. The dotted line in the phase diagram roughly corresponds to this location.

We stress that in this way we are actually able to predict a surface phase transition of a continuous Lennard-Jones system, and to identify this transition as roughening, whereas determination of the nature of the transition is not possible in direct Monte Carlo or Molecular Dynamics calculations on the continuous system.

Zhu and Dash³ performed heat capacity measurements on thick Argon films adsorbed on graphite. They observed, apart from surface melting, weak, rounded anomalies at $T = 68$ K, which they identified tentatively as roughening. Roughening is accompanied by a small peak in the heat capacity, which lies somewhat below the actual roughening temperature T_R . Our value $T_R = 70.5 \pm 0.5$ K is in good agreement with the peak in the heat capacity at $T = 68$ K.

Van der Eerden *et al.*⁶ performed Monte Carlo simulations on the (001) face of a Lennard-Jones fcc structure, and observed the vanishing of the surface shear modulus at $T = 64 \pm 2$ K. Regarding the difficulties in determining this temperature, due to the fact that the way in which the shear modulus vanishes is not known, and judging from their figures, we find the roughening temperature T_R as found by us in correspondence with their findings.

V. CONCLUSIONS

We studied the (001) face of a Lennard-Jones fcc structure, particularly pertaining to Argon. Direct Monte Carlo or Molecular Dynamics simulations of such systems do indicate the presence of surface phase transitions, but cannot unambiguously determine the nature of such a transition; the appropriate way to do so is to use a discrete lattice model. Therefore we provided for a link between the continuous Lennard-Jones system and the corresponding lattice model, which is, in this case, a BCSOS model. We describe a method to calculate the effective interaction constants in the lattice model, arising from the Lennard-Jones interaction, and carried out the calculations for (001) surface. We observed that entropy effects, arising from the gain in freedom of an atom adjacent to a vacancy, considerably lower the interaction constants. The BCSOS model is shown to exhibit a roughening transition at $T = 70.5 \pm 0.5$ K, which is in good agreement with experimental results for Argon.

Several checks on the approximations used for the calculations are dealt with in the Appendix. We note that the approximations allow for an estimate of their accuracy. In this way one can, when more accurate numerical data are required, give a quantitative estimate of the effect of the approximations and build in corrections.

The method described in this paper can be applied to other systems and other surfaces as well. For the (110) surface of an fcc structure, the same BCSOS model applies, albeit with different values of the couplings. We stress that the phase diagram of the BCSOS model shows, apart from a flat and a rough phase, also a Disordered Flat phase. It may be possible, applying the method for the (110) surface, to determine a preroughening transition from the flat into the Disordered Flat phase.

In the case of the (001) face of a fcc Lennard-Jones system, surface melting, a disordering of the surface layers judged from correlation functions, layer occupation etc., is shown to be

accompanied by a genuine surface phase transition, which is a roughening transition in this particular case. A precise, atomic-scale definition of surface melting is required to further examine the interplay between the disordering process and the possibility of surface phase transitions.

ACKNOWLEDGMENTS

We thank Jan van der Eerden for discussions and for providing the program SIMLIB, used to carry out the Monte Carlo simulations.

APPENDIX:

Several additional calculations, validating the approximations we made, have been performed and will be treated in this Appendix. The most important approximations arise from the transition from three dimensional to two dimensional, and from the reduction of the number of points in a cell.

1. Free energy of the bulk

First we want a general check on all approximations. The method we followed for calculating the surface free energies, including all approximations, can also be used for calculating the free energy of the bulk and consequently the vapor pressure, which can be compared with experimental values for Argon. We do this as follows. Consider a (001) layer in the bulk. This layer is subject to two substrate potential patterns as calculated in Sec. III A; one from below, and one from above. These two potential patterns are exactly those we calculated already. Using those two patterns as the potential pattern in a bulk (001) layer, we can apply the transfer matrix to obtain the bulk free energy. The bulk free energy is then obtained using all approximations we used for calculating the surface free energy, that is, treating the potential pattern in a mean field approximation, treating the cells as two-dimensional and drastically reducing the number of grid points in the cell.

The full partition function of the bulk system consisting of N atoms is

$$Z_{\text{bulk}} = \frac{1}{h^{3N}} \int d^3 \mathbf{p}_j \exp\left(-\frac{\beta \mathbf{p}^2}{2m}\right) Z_{\text{conf}}, \quad (\text{A1})$$

where h is Planck's constant. Note that we do not need correct Boltzmann counting; the particles can be identified by their cells. The first part of this expression is the trivial kinetic part of the energy, the second part is the configurational part which equals

$$Z_{\text{conf}} = \lambda_{\text{max}}^{N/3}, \quad (\text{A2})$$

where λ_{max} is the largest eigenvalue of the transfer matrix with the bulk potential pattern. Note that this eigenvector pertains two a row with three atoms in it; hence the factor $N/3$. Note also that $\lambda_{\text{max}}^{1/3}$ has the dimension of a volume.

The kinetic part of Eq. (A1) is easily integrated. Substituting the appropriate values (Argon has a mass of 39.948 atomic units), gives the Helmholtz free energy which equals the Gibbs free energy G because $P = 0$, so

$$\frac{\beta G}{N} = -\frac{3}{2} \ln \left(\frac{2\pi m}{\beta h^2} \right) - \frac{1}{3} \ln \lambda_{\max}. \quad (\text{A3})$$

The Gibbs free energy per particle equals the chemical potential μ . The vapor, being very sparse, behaves as an ideal gas and has a chemical potential μ ,

$$\beta \mu = \ln(\lambda^3 \beta P), \quad (\text{A4})$$

where P is the vapor pressure and λ the thermal wavelength,

$$\lambda = \sqrt{\frac{h^2 \beta}{2\pi m}}. \quad (\text{A5})$$

We plot the Gibbs free energy together with the experimental values,²⁵ calculated from the vapor pressure, in Fig. 11. Regarding the fact that all approximations are present in the plot, the correspondence is remarkable.

2. Cluster calculations

We will now check the error arising from going from a three dimensional, dense grid of points to a two dimensional grid consisting of 25 points in the cells. We use a cluster calculation of a small configuration of particles at the surface. In this configuration, we fix all particles at their equilibrium positions, except for one. This particle is moving through its cell in the field of the others. We choose the two configurations depicted in Fig. 12; in Fig. 12(a) all cells are occupied, in Fig. 12(b) there is a step present. The central particle in both of the figures is the particle that moves.

We calculate the free energy of both configurations in two ways: the first using the full three dimensional potential pattern consisting of $21 \times 21 \times 21$ points. In the second calculation, the pattern is first averaged over its vertical coordinate, thus consisting of 21×21 points. To obtain an indication of the step free energy, we divide the potential by two, as it should in a cluster calculation. Results are plotted in Fig. 13, showing that the averaging hardly has any effect. Note that the difference between the two plots (a) and (b) indicates the step free energy. Compare this with the step free energies plotted in Fig. 5, notably the values for F_1 . It follows that a cluster calculation still overestimates the step energy.

Next we test the effect of sparsing the grid. We calculate the free energy of the configuration in Fig. 12(a), but now using the transfer matrix with the grid consisting of 25 points. For comparison, we plot the results together with the exact calculation. The plot is shown in Fig. 14, showing that sparsing the grid is a reasonable approximation. Note that we used the full potential in this calculation, whereas the calculation from Fig. 13 is done with the potential divided by two.

We conclude, from both checks, that within a reasonable accuracy, the approximations used are valid.

REFERENCES

- * e-mail paulb@tvs.kun.nl.
- ¹ R. Lipowsky, Phys. Rev. Lett. **49**, 1575 (1992); R. Lipowsky and W. Speth, Phys. Rev. B **28**, 3983 (1983).
- ² For a review, see H. Löwen, Phys. Rep. **237**, 249 (1994).
- ³ D. Zhu and J. G. Dash, Phys. Rev. Lett. **57**, 2959 (1986).
- ⁴ J. P. van der Eerden, A. Roos, and J. M. van der Veer, J. Cryst. Growth **99**, 77 (1990).
- ⁵ J. P. van der Eerden, H. J. F. Knops, and A. Roos, J. Chem. Phys. **96**, 714 (1992).
- ⁶ J. P. van der Eerden, T. H. M. van den Berg, J. Huinink, and H. J. F. Knops, J. Cryst. Growth **128**, 57 (1993).
- ⁷ B. I. Halperin and D. R. Nelson, Phys. Rev. Lett. **41**, 121 (1978); E **41** 519 (1978).
- ⁸ D. R. Nelson and B. I. Halperin, Phys. Rev. B **19**, 2457 (1979).
- ⁹ A. P. Young, Phys. Rev. B **19**, 1855 (1979).
- ¹⁰ For a review, see K. J. Strandburg, Rev. Mod. Phys. **60**, 161 (1988).
- ¹¹ J. V. José, L. P. Kadanoff, S. Kirkpatrick, and D. R. Nelson, Phys. Rev. B **16**, 1217 (1977).
- ¹² J. Q. Broughton and G. H. Gilmer, J. Chem. Phys. **79**, 5105, (1983); **79**, 5119 (1983).
- ¹³ M. Bernasconi and E. Tosatti, Surf. Sci. Rep. **17**, 363 (1993).
- ¹⁴ H. van Beijeren and I. Nolden, in *Structure and Dynamics of Surfaces II*, edited by W. Schommers and P. Von Blanckenhagen (Springer, Heidelberg, 1987).
- ¹⁵ K. Rommelse and M. den Nijs, Phys. Rev. Lett. **59**, 2578 (1987); M. den Nijs and K. Rommelse, Phys. Rev. B **40**, 4709 (1987).
- ¹⁶ J. Villain and I. Vilfan, Surf. Sci. **199**, 165 (1988); I. Vilfan and J. Villain, Surf. Sci. **257**, 368 (1991).
- ¹⁷ J. Q. Broughton and G. H. Gilmer, J. Chem. Phys. **84**, 5749 (1986).
- ¹⁸ P. Flubacher, A. J. Leadbetter, and J. A. Morrison, Proc. Phys. Soc. London **78**, 1449 (1961).
- ¹⁹ H. van Beijeren, Phys. Rev. Lett. **38**, 993 (1977).
- ²⁰ P. J. M. Bastiaansen and H. J. F. Knops, Phys. Rev. B (to be published).
- ²¹ J. Q. Broughton and G. H. Gilmer, J. Chem. Phys. **79**, 5095 (1983).
- ²² See, e.g., R. J. Baxter, *Exactly solved models in statistical mechanics* (Academic Press, New York, 1982).
- ²³ See, e.g., P. Nightingale, J. Appl. Phys. **53**, 7927 (1982).
- ²⁴ M. den Nijs, Phys. Rev. Lett. **64**, 435 (1990).
- ²⁵ Handbook of Chemistry and Physics, 62nd edition, Eds. R. C. Weast and M. J. Astle, CRC Press Florida (1981-1982).

TABLES

TABLE I. Comparison of the vertex free energies F_j in units of kT at $T = 50$ K and $T = 70$ K. The second and third columns show the actual free energies of the vertices 1 to 4. In the fourth column, the same free energies are calculated, but now using the potential pattern at $T = 50$ K scaled to the cell dimensions of $T = 70$ K. The last column shows the relative contribution of the increased cell dimensions to the total effect. It follows that the decrease of free energy with increasing temperature is for roughly 98% due to the increasing cell dimensions, and for 2% to the flattening potential pattern.

Vertex number	50 K	70 K actual	70 K scaled	%
1	1.4180	0.8133	0.8219	98.6
2	1.1322	0.6314	0.6390	98.5
3	0.9814	0.5048	0.5130	98.3
4	1.6028	0.7848	0.8018	97.9

FIGURES

FIG. 1. Four different step configurations at a vertex. Shaded cells are occupied, white cells are empty. Thick lines are the oriented steps at the vertex configuration. F_j denotes the free energy. Note that the configurations are rotationally invariant, so F_1 represents four different configurations. The empty configuration, without step, is not shown and has a free energy $F = 0$.

FIG. 2. The nearest neighbor distance of the Argon fcc crystal against temperature. The solid line is a polynomial fit of our results, the dashed line is that of Broughton and Gilmer. Note the y -scale.

FIG. 3. Distribution of points in a cell. There are 25 points in the cell, each one in its corresponding domain. The potential in each of the domains is averaged, its Boltzmann weight is calculated and multiplied by the area of the domain. The points are in the middle (the ‘center of mass’) of the domain, and the domains are uniquely defined according to the parameters R_1 , R_2 and ϕ . Note that symmetry is that of a square. The parameters are fixed such that the Boltzmann weights multiplied by the corresponding area are all equal, in order to obtain a distribution which is as efficient as possible.

FIG. 4. Nine surface configurations. The squares are the cells in which the surface atoms move, empty squares denoting empty cells and shaded squares denoting occupied cells. Each of the surface configurations is understood to extend to infinity on both sides. Steps on the surface (that is, borders between empty and occupied cells) make up closed oriented loops, and are indicated with thick lines.

FIG. 5. Free energies F_1 to F_4 of the four different vertex configurations of Fig. 1. Symbols: \diamond straight step, $+$ inside corner, \square outside corner, \times crossing. The temperature dependence of the crossing of two steps is the strongest, which means that there the entropy plays a more important role.

FIG. 6. Free energy of surface configuration number 7 from Fig. 4. Symbols: \square is the calculated free energy, $+$ is the energy in terms of broken bonds, and \triangle is the free energy calculated from the vertex free energies F_j from Fig. 1. It follows that expressing the free energy of the surface in terms of the vertex free energies is accurate; \square and \triangle are approximately the same. Also follows that calculating the energy of a surface configuration by counting the broken bonds considerably overestimates the actual value; the figure shows that a substantial entropy effect is present. As expected, this effect gets stronger with increasing temperature.

FIG. 7. Typical surface configuration for a (001) surface of an fcc crystal. The circles are the atoms, darker circles representing atoms that are higher on the surface. Neighboring atoms always differ half a lattice distance in height. The six vertex lattice is depicted with thin, solid lines and small arrows. The thick solid line is a step on the surface, and indicates a height difference of one lattice distance a between next nearest neighbors.

FIG. 8. The six possible arrow combinations at a vertex of the six vertex model. The six vertex model can be mapped onto a surface model by assigning heights to each of the lattice sites. Looking in the direction of the arrow, the higher atom is on the right. The thick arrows denote height differences between next nearest neighboring atoms, and form a closed, oriented loop on the surface. The loop corresponds to a step.

FIG. 9. Different elementary surface configurations. Compare Fig. 7, and note that the lattice is tilted over 45° . The thin solid lines make up the six vertex lattice, each bond carrying an arrow and indicating a height difference $\pm\frac{1}{2}a$ between adjacent atoms. Heights, in terms of the lattice parameter a , are indicated on the sites. The interaction is defined on the central side. For convenience also the adjacent sites are depicted. The four vertices represented as \bullet take part in the interaction, but only insofar their arrows are depicted. Thick lines are steps on the surface, indicating a height difference between next nearest neighbor atoms. (a) is the flat configuration carrying no step, (b) is a straight step, (c) is a corner and (d) is a crossing. The free energy of (a) is 0, of (b) is F_1 , of (c) is $(F_2 + F_3)/2$, and of (d) is F_4 . Note that we do not distinguish between inside and outside corners.

FIG. 10. The phase diagram of the BCSOS model. The parameters W and K are the Boltzmann weights assigned to a broken next nearest neighbor bond and a broken third nearest neighbor bond respectively. The model exhibits flat, rough, Disordered Flat (DOF) and reconstructed phases as indicated. The dotted line roughly corresponds to the path the Agorn (001) surface is following as a function of temperature.

FIG. 11. Gibbs free energy of solid Argon. The dashed line is calculated from the experimentally known vapor pressure, the solid line is calculated using the transfer matrix method described in the text.

FIG. 12. Two surface configurations used for a cluster calculation. Symbols: \bullet are atoms fixed in the center of their cells, \circ are the atoms that move. (a) is a fully occupied surface, (b) is a surface with a step. The rightmost cells of (b) are empty.

FIG. 13. Free energy of the clusters depicted in Fig. 12, calculated in two different ways. (a) free energy of the fully occupied configuration from Fig. 12(a), (b) is from the configuration with a step in Fig. 12(b). Symbols: solid lines and \square are calculated using the full three dimensional potential pattern, dashed lines and \diamond are the results after averaging the potential pattern over its vertical coordinate.

FIG. 14. Free energy of the cluster depicted in Fig. 12(a). Solid lines with \square are the exact results, using the potential pattern defined on a fine grid of $21 \times 21 \times 21$ points. The dashed line with $+$ is the result from a transfer matrix calculation, using a two dimensional grid consisting of 25 points.

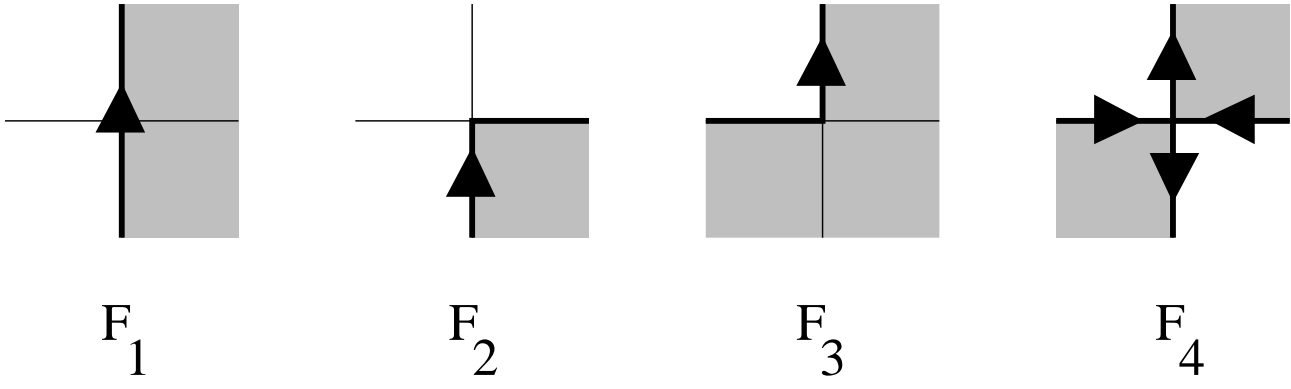


Figure 1

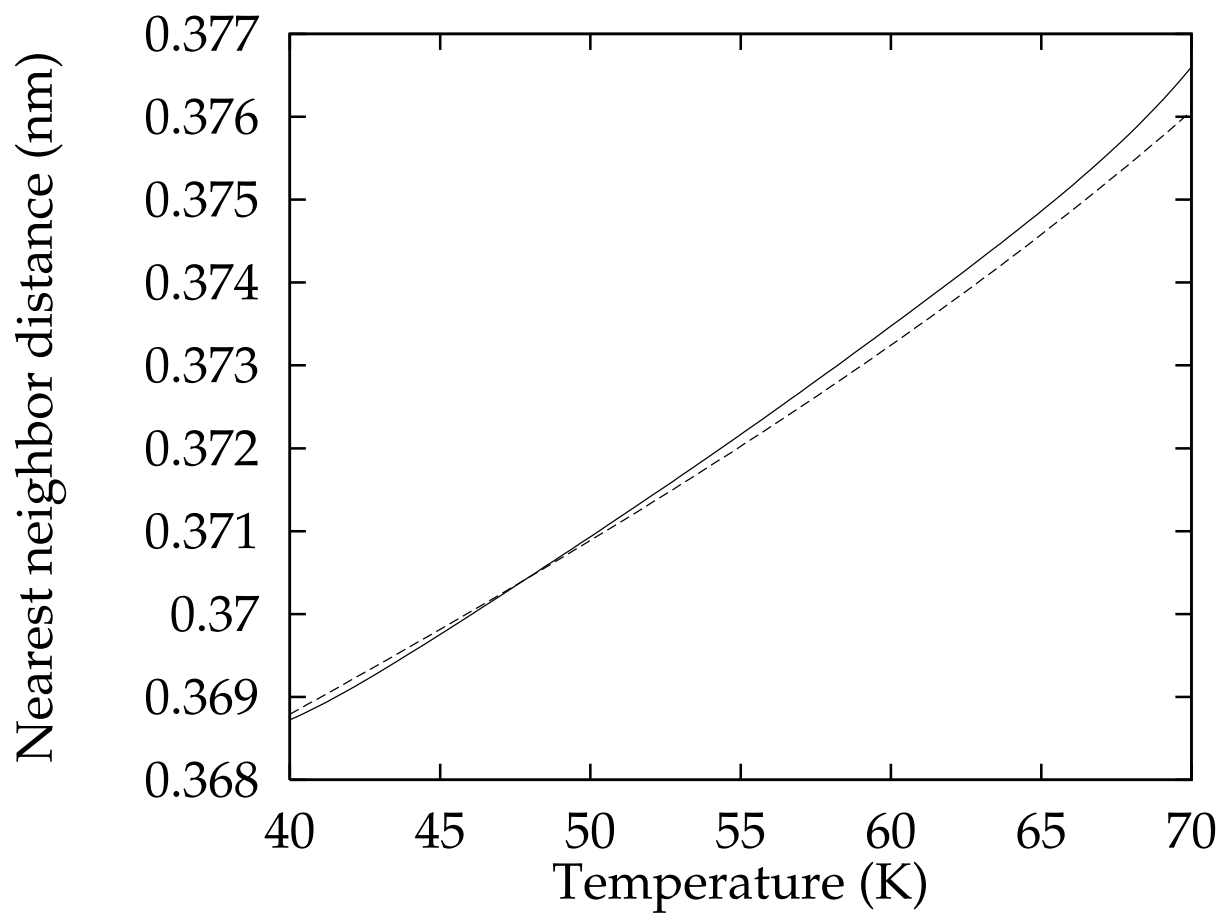


Figure 2

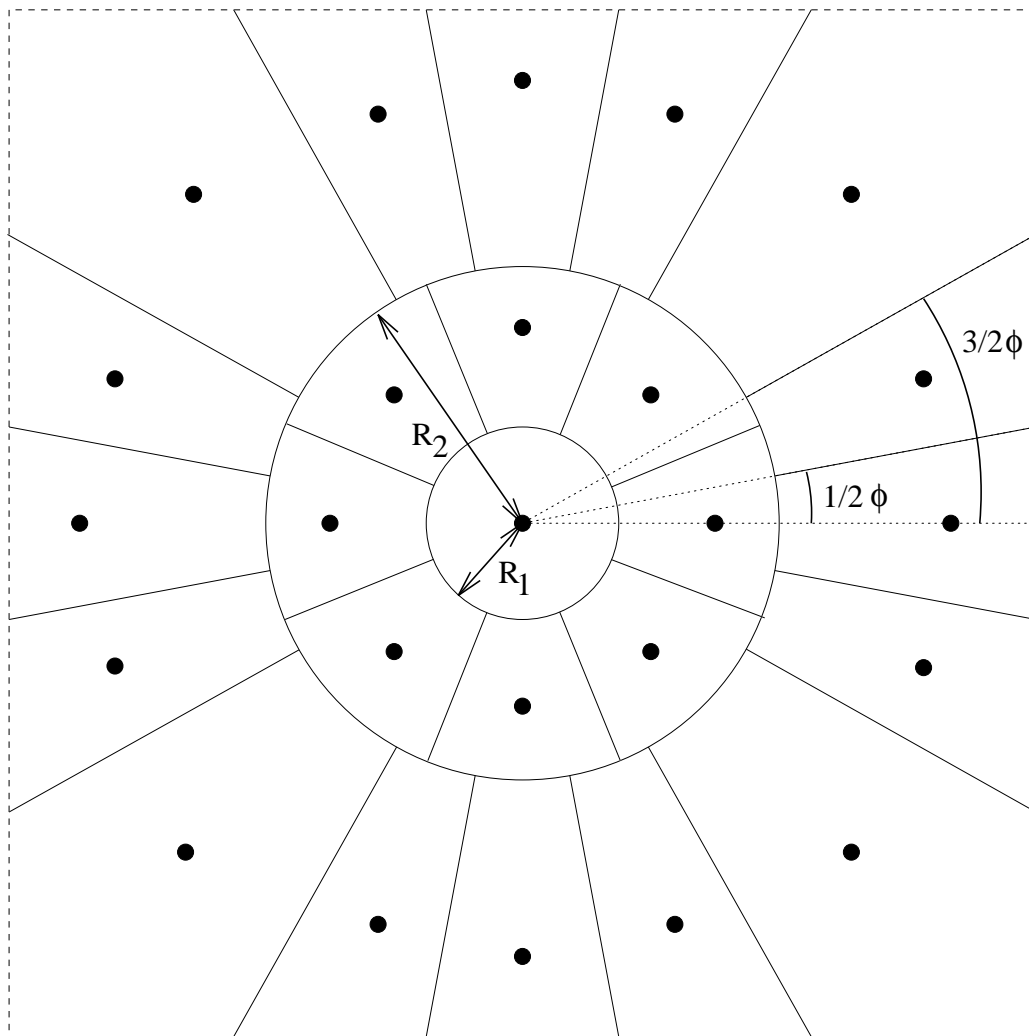


Figure 3

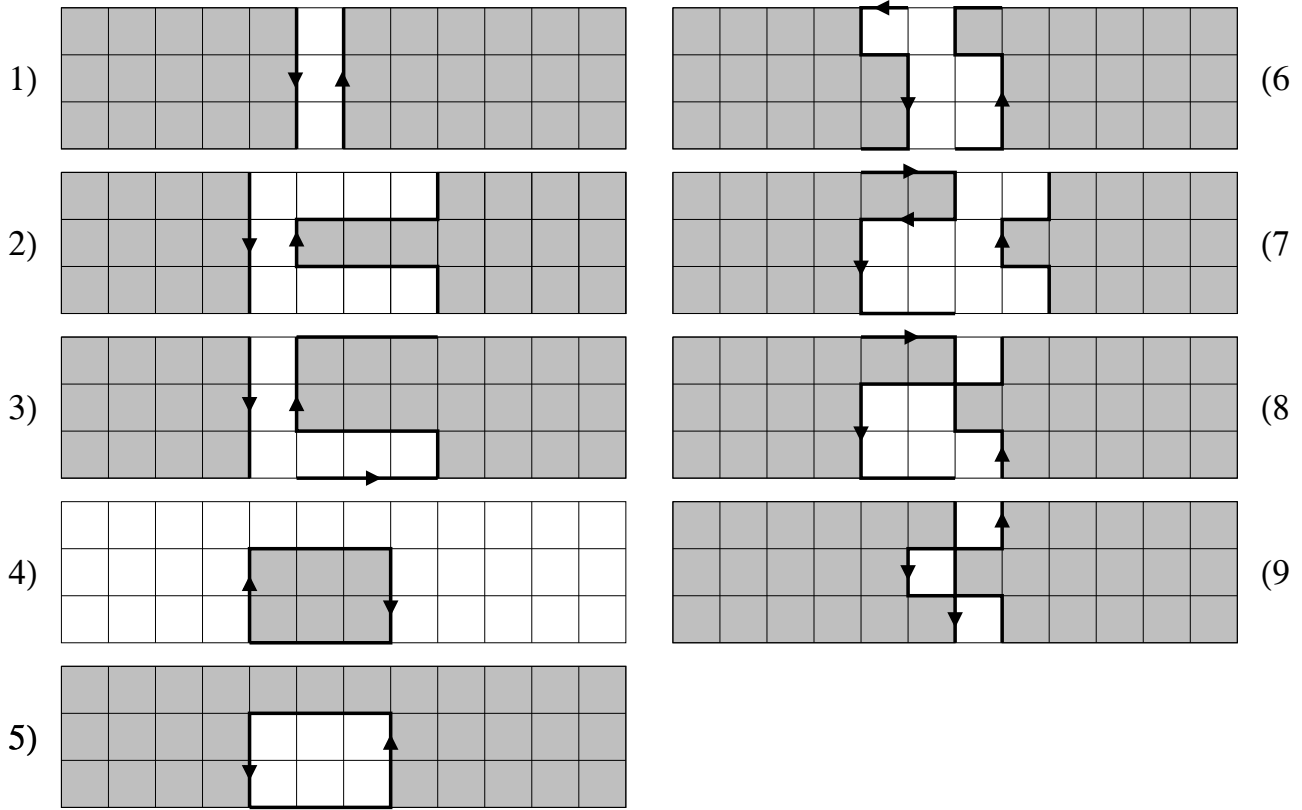


Figure 4

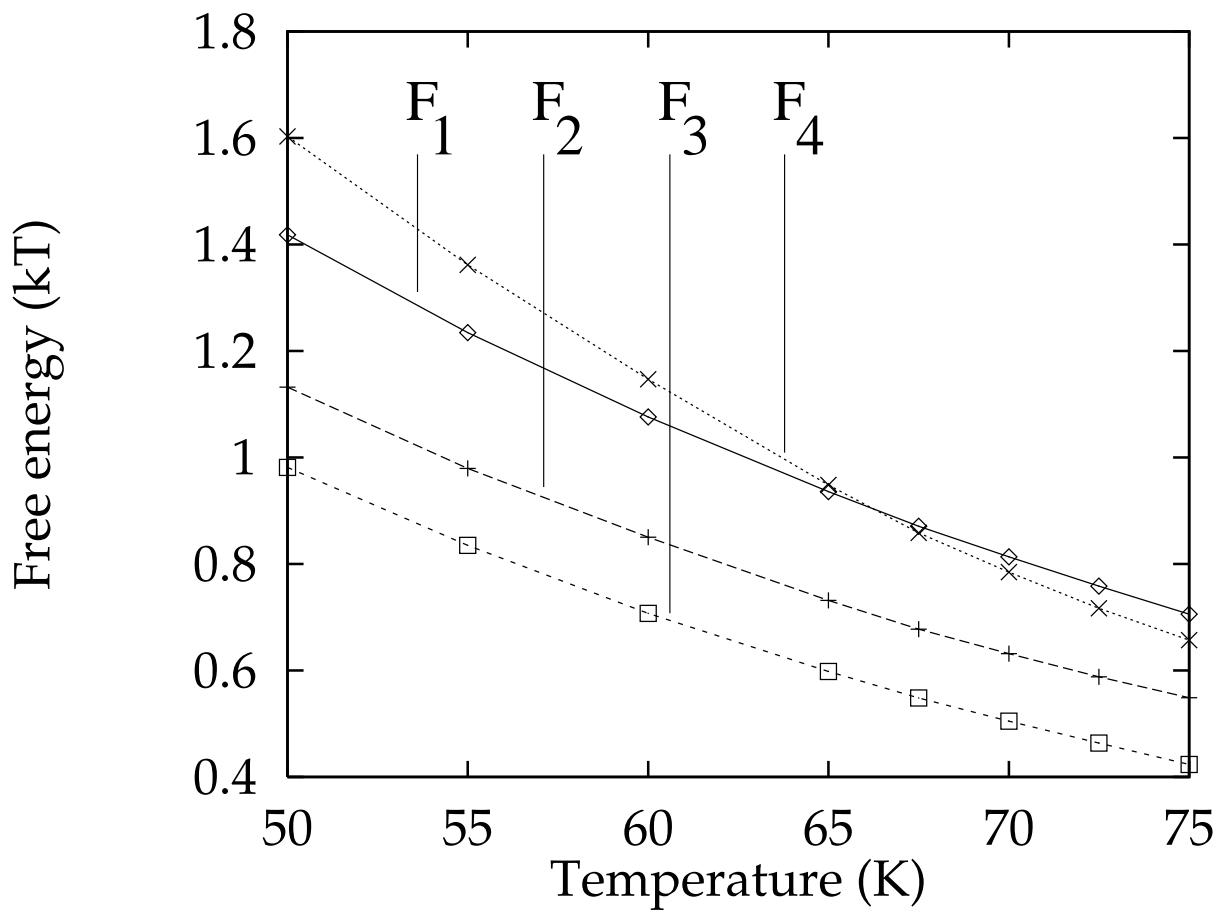


Figure 5

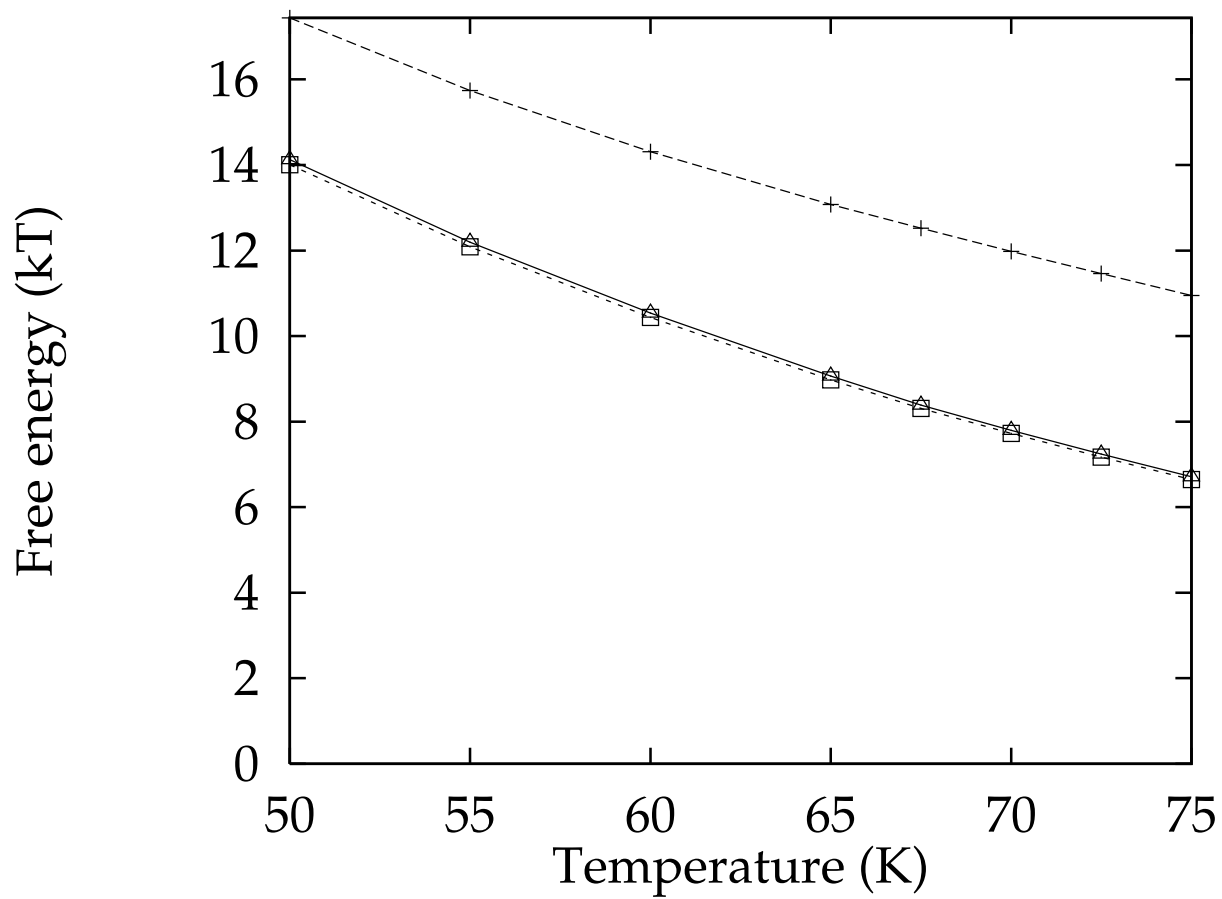


Figure 6

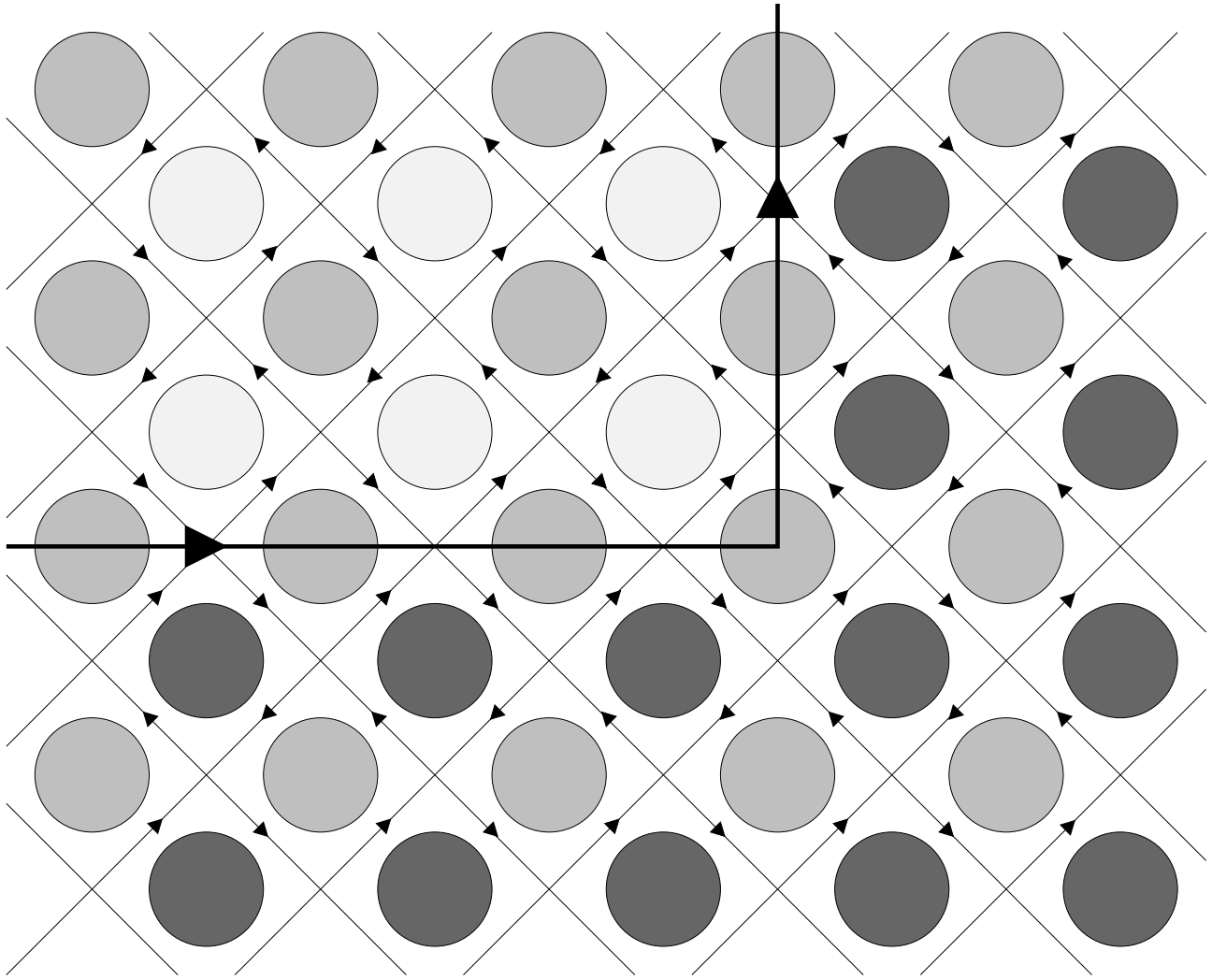


Figure 7

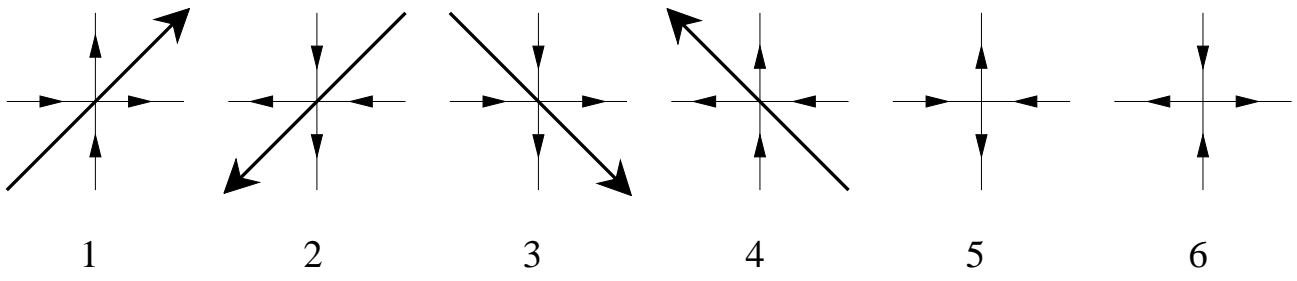


Figure 8

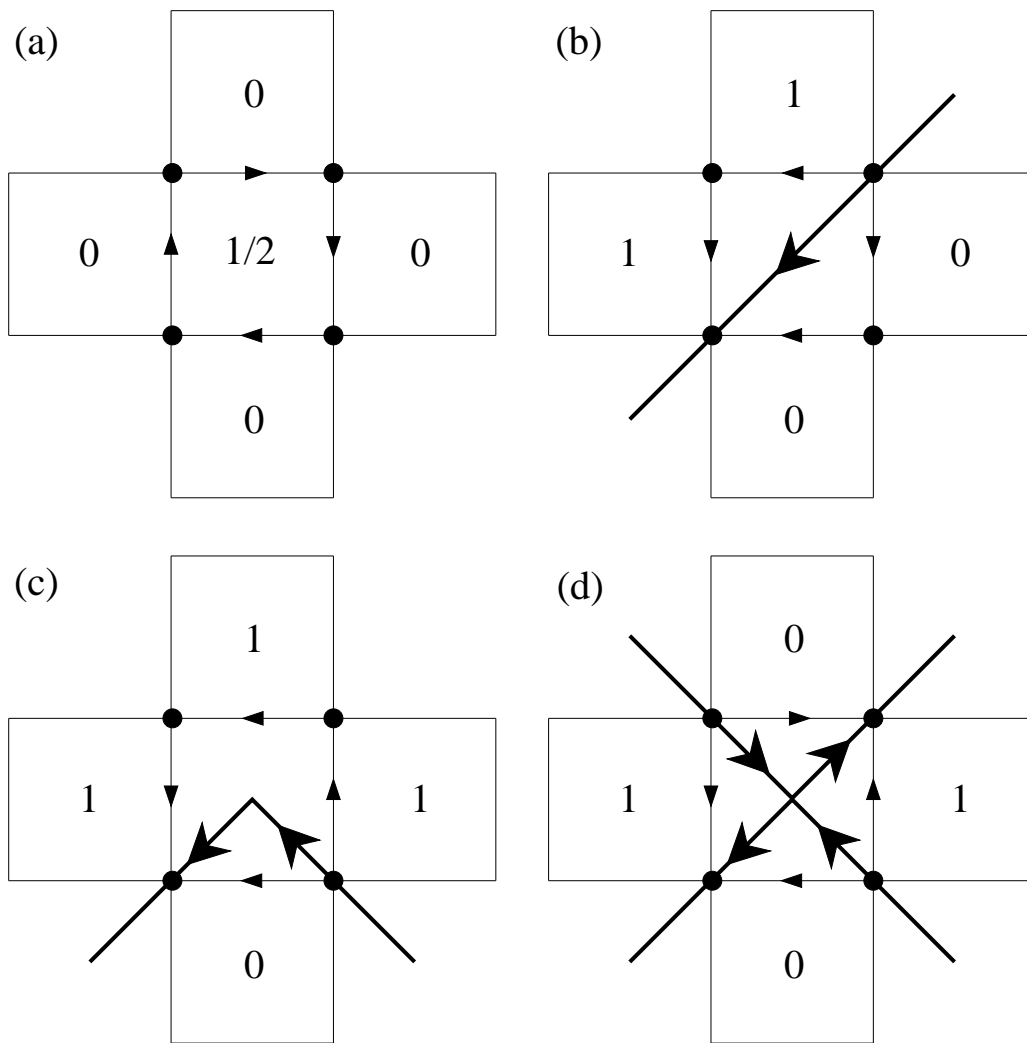


Figure 9

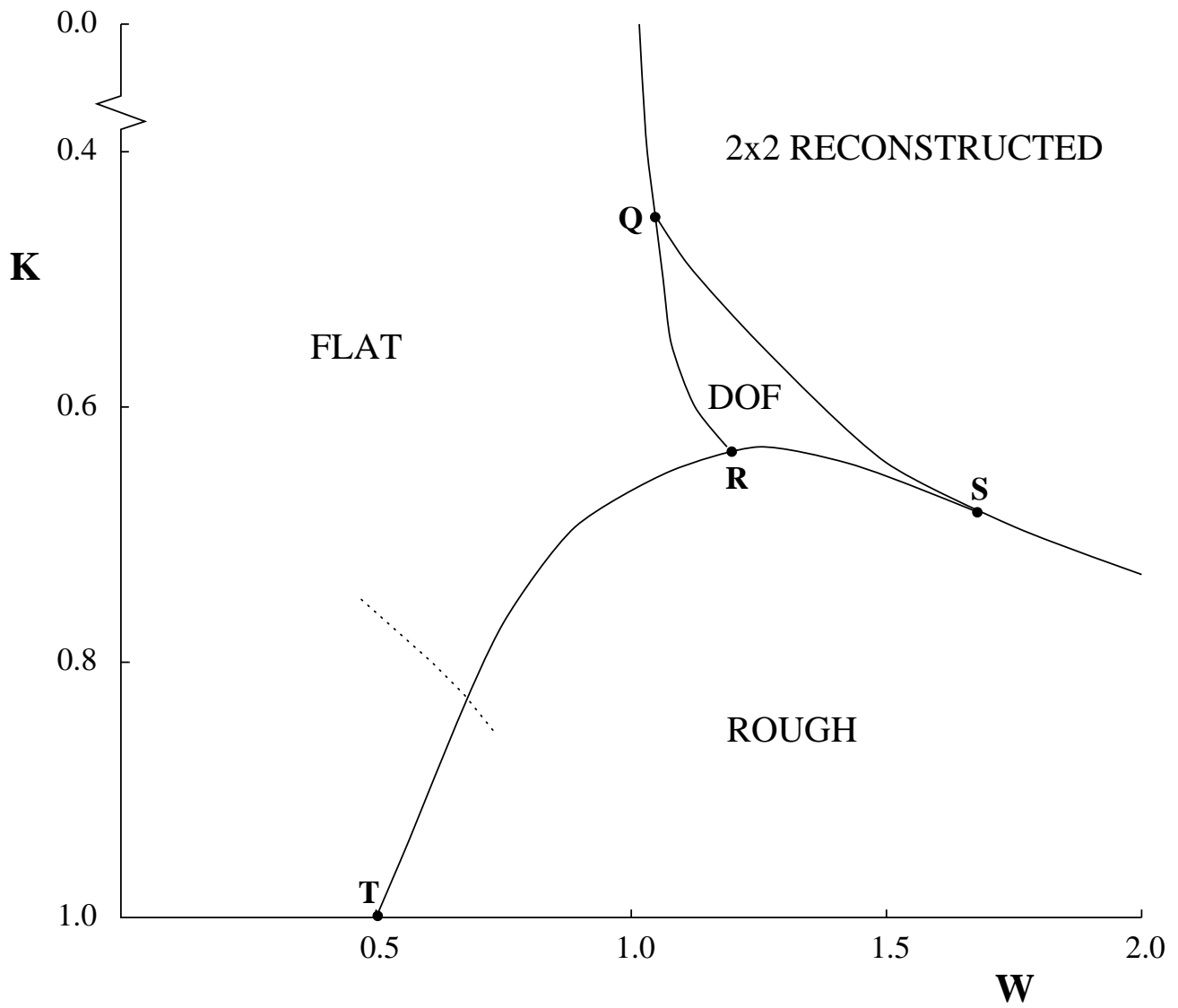


Figure 10

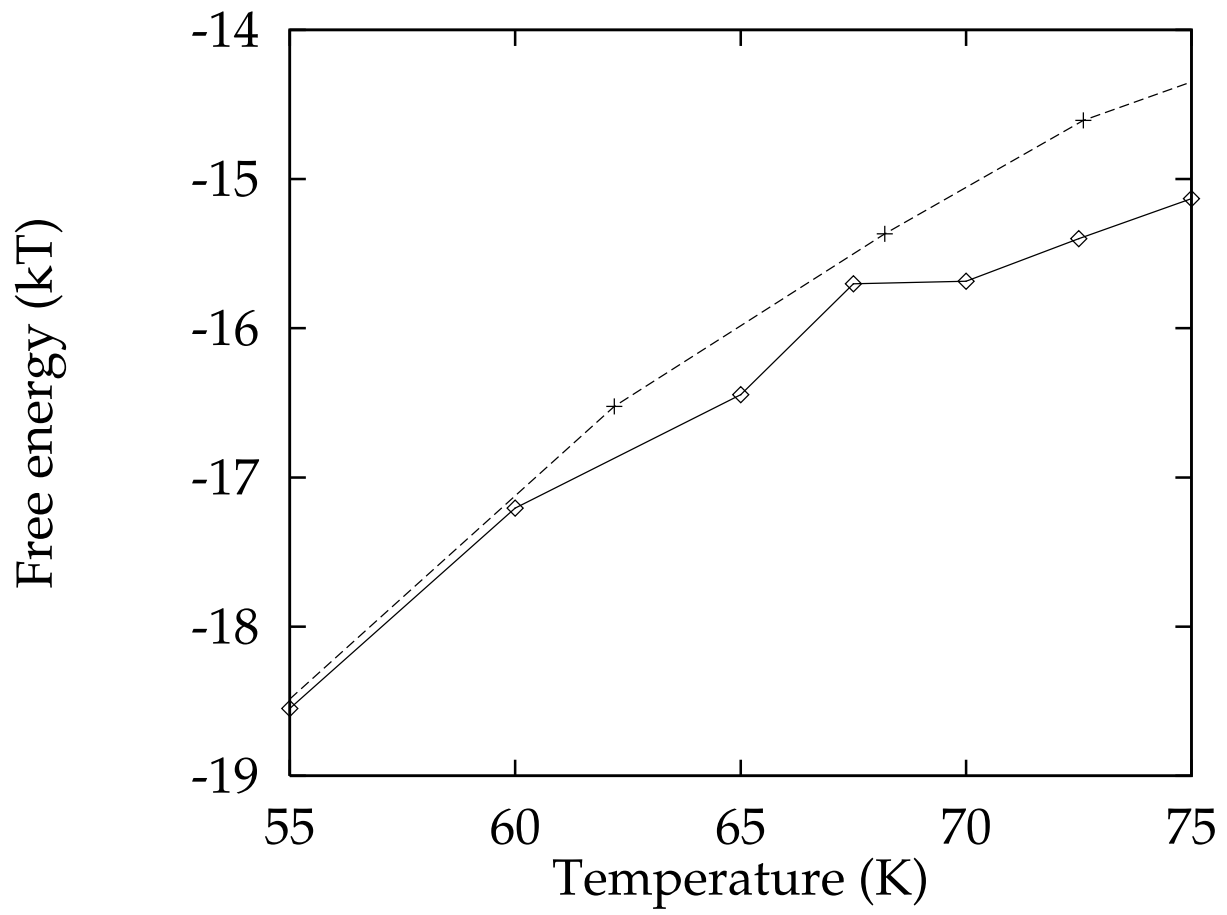
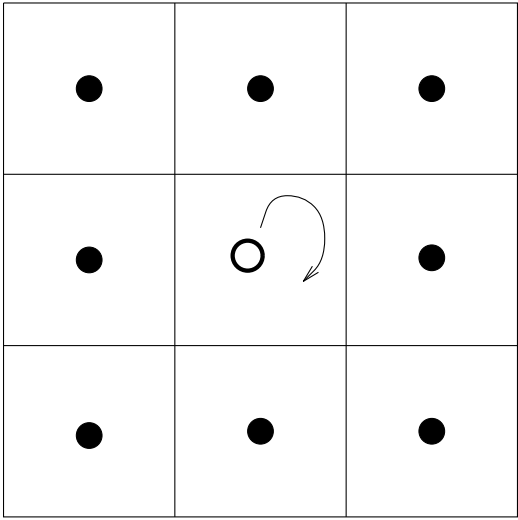
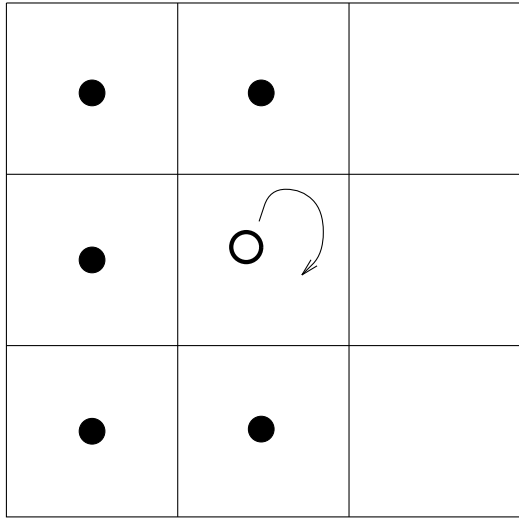


Figure 11



(a)



(b)

Figure 12

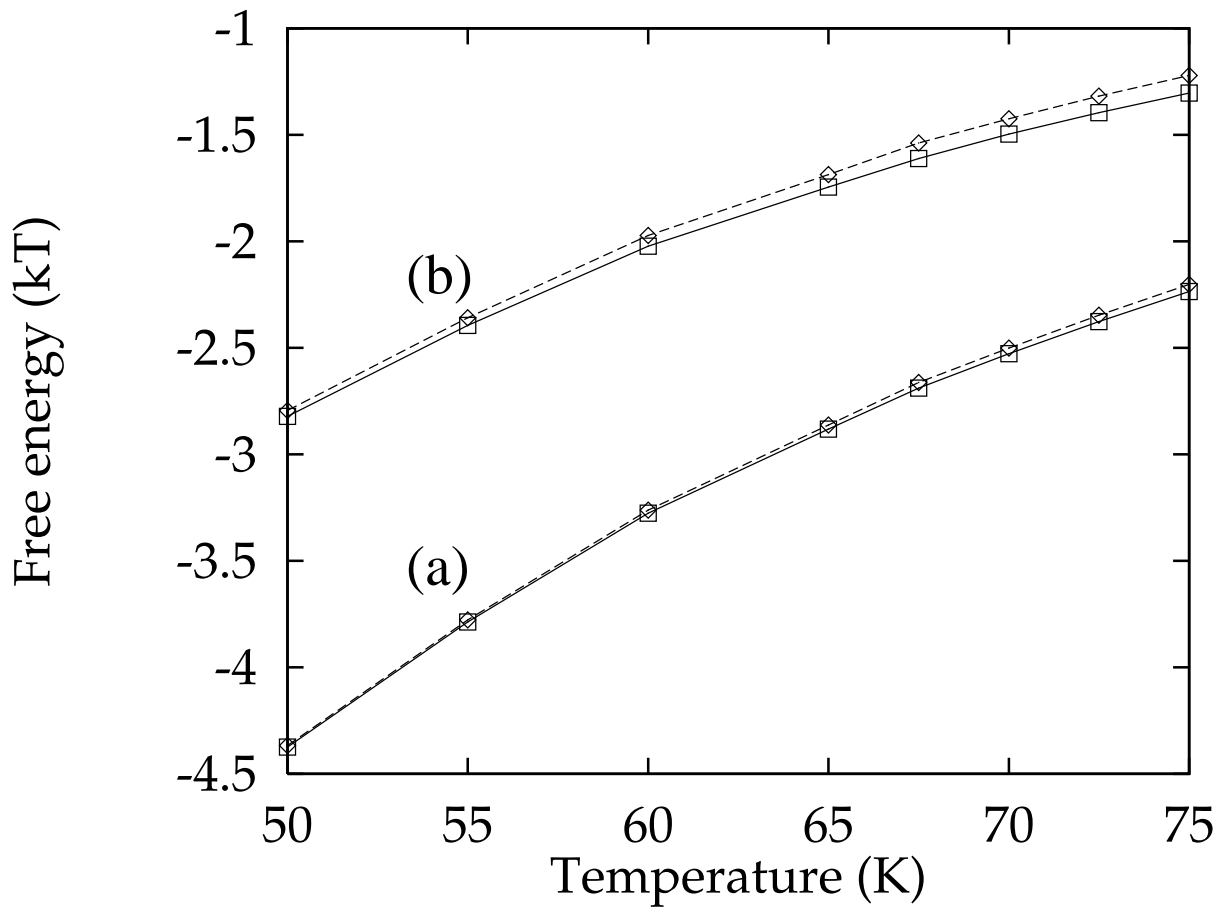


Figure 13

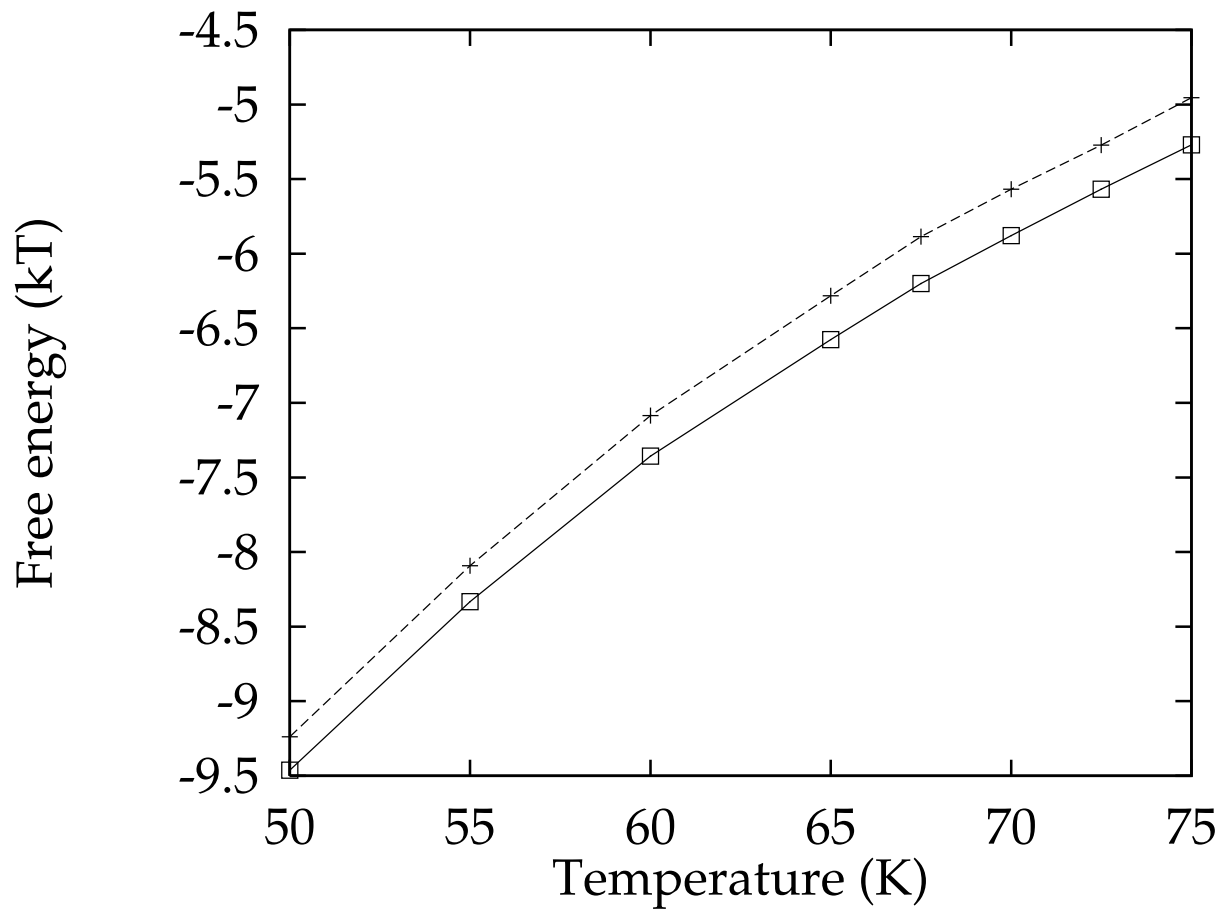


Figure 14